

Open Vocabulary Monocular 3D Object Detection

Jin Yao¹ Hao Gu¹ Xuweiyi Chen¹ Jiayun Wang² Zezhou Cheng¹
¹ University of Virginia ² California Institute of Technology
<https://cvlab.cs.virginia.edu/ovmono3d>

Abstract

In this work, we pioneer the study of open-vocabulary monocular 3D object detection, a novel task that aims to detect and localize objects in 3D space from a single RGB image without limiting detection to a predefined set of categories. We formalize this problem, establish baseline methods, and introduce a class-agnostic approach that leverages open-vocabulary 2D detectors and lifts 2D bounding boxes into 3D space. Our approach decouples the recognition and localization of objects in 2D from the task of estimating 3D bounding boxes, enabling generalization across unseen categories. Additionally, we propose a target-aware evaluation protocol to address inconsistencies in existing datasets, improving the reliability of model performance assessment. Extensive experiments on the Omni3D dataset demonstrate the effectiveness of the proposed method in zero-shot 3D detection for novel object categories, validating its robust generalization capabilities. Our method and evaluation protocols contribute towards the development of open-vocabulary object detection models that can effectively operate in real-world, category-diverse environments.

1. Introduction

Recognizing objects from a single image has been a long-standing task in computer vision, with broad applications in robotics and AR/VR. Over recent decades, 2D object detection — identifying and localizing objects within a 2D image plane — has achieved substantial progress, driven by advancements in deep learning techniques [9, 16, 20, 44] and large annotated datasets [19, 31, 49]. However, recognizing only a fixed set of objects is limiting, given the vast diversity of objects in real-world settings; detecting objects solely in 2D space is also insufficient for most practical tasks, as the world and its objects exist in 3D space.

To address these challenges, one line of recent research has focused on open-vocabulary 2D object detection [12, 32, 55, 65] (Fig. 1b) to identify objects beyond a fixed set of categories. Another line explores the monoc-

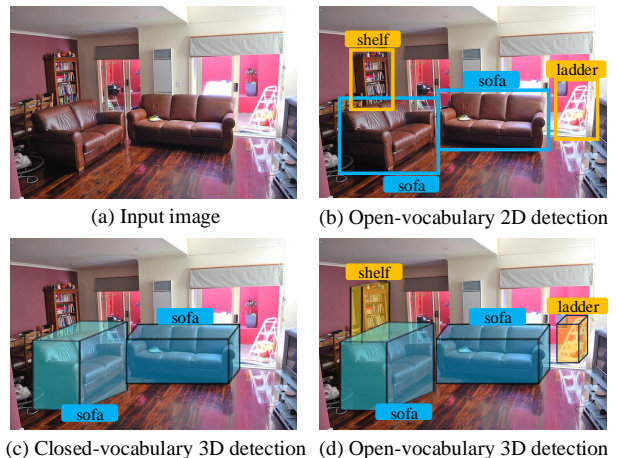


Figure 1. Given (a) a single image, we illustrate examples of (b) open-vocabulary 2D detection, which localizes objects of any category within the 2D image plane, covering both **seen** categories and **novel** categories not seen during training; (c) closed-vocabulary 3D detection, which detects objects from a predefined set of categories in 3D space; and (d) open-vocabulary 3D object detection, which identifies objects of any category in 3D.

ular 3D detection task [5, 37, 47, 53] (Fig. 1c), which extends detection capabilities from 2D to 3D space. Despite the vast research in these two lines of research, the intersection of these two areas — open-vocabulary monocular 3D detection, referred to as OVMONO3D (Fig. 1d) — remains largely unexplored.

In this work, we aim to fill this gap. The OVMONO3D task involves detecting and localizing objects of any categories in the metric 3D space, including novel categories unseen during training. We identify two primary challenges in this task: first, the lack of a well-defined task setting and standardized evaluation protocol, which complicates consistent model assessment; and second, the scarcity and limited quality of labeled 3D data, as annotating detailed 3D bounding boxes is labor-intensive (Fig. 2 and Fig. 3).

To address these challenges, we first propose a formal definition of the task and a simple protocol to mitigate the impact of annotation issues (*e.g.*, missing labels) in evalu-

ations (Sec. 3). Our evaluation metric enables direct performance assessment without exhaustive 3D annotations, which is especially useful for efficient real-world evaluation of a detection system, where annotating every object is impractical and error-prone.

One unique challenge in OVMONO3D is the lack of large-scale 3D datasets with high-quality annotations (Fig. 2). For this reason, we adopt an approach that decouples the tasks of recognizing and localizing objects in 2D from estimating their 3D bounding boxes. We first consider a simple training-free method which un-projects 2D detections from off-the-shelf open-vocabulary 2D detectors [12, 32] into 3D via geometric principles, referred to as OVMONO3D-GEO (Fig. 4a). Despite of its simplicity and effectiveness in general cases, we find this approach lacks of robustness to object occlusion.

To tackle this issue, we then introduce a data-driven approach, OVMONO3D-LIFT, which learns to lift 2D detections to 3D (Fig. 4b). We comprehensively explore its design space, examining choices such as network backbones, 2D base detectors, and dataset size. Our experiments show that OVMONO3D-LIFT achieves state-of-the-art performance in detecting novel objects in 3D, and demonstrates strong generalization on in-the-wild images (Fig. 7).

We summarize our contributions as follows:

- We conduct the first comprehensive study on open-vocabulary monocular 3D object detection, formally define the task and evaluation metrics, and extensively explore the design space of several baseline methods.
- The proposed OVMONO3D-LIFT effectively decouples the tasks of 2D recognition and localization from 3D spatial estimation, achieving superior performance compared to alternative baseline methods.
- We provide an in-depth analysis of design choices and demonstrate the effectiveness of our approach in zero-shot monocular 3D detection on in-the-wild images.

2. Related Work

Open-Vocabulary 2D Object Detection. The goal of this task is to recognize and localize objects in 2D images beyond a fixed set of predefined categories. Leveraging large-scale 2D datasets [25, 39, 49], this field has seen considerable advancement. Some approaches [18, 35, 36, 57] employ pre-trained vision-language models [24, 41], using frozen text features to detect novel categories. Other methods [12, 28, 32, 60] are pre-trained on extensive detection, grounding, and caption data to align region-text features. For example, Grounding DINO [32] incorporates grounded pre-training with cross-modal feature fusion, while YOLO-World [12] uses region-text contrastive loss and re-parameterization to enhance both accuracy and efficiency. However, such large-scale annotations are costly

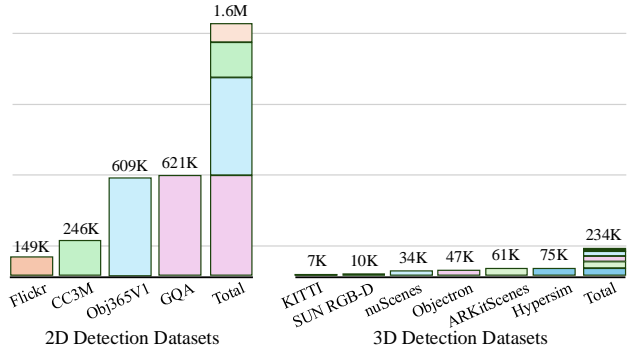


Figure 2. **2D vs. 3D Detection Datasets in terms of #Images.** Due to the challenges of 3D annotation, publicly available 3D datasets with 3D annotations are significantly smaller than 2D detection datasets

in 3D detection; thus, we investigate methods to adapt existing open-vocabulary 2D detectors for 3D detection.

Open-Vocabulary 3D Object Detection. This task seeks to identify objects from any category in 3D, including those unseen during training. Prior research [7, 8, 33, 34, 40, 58, 61, 63, 70] primarily focuses on 3D detection tasks with 3D point clouds as input. [33] first proposes an open-vocabulary 3D detector using image-level class supervision from ImageNet1K [48]. [34] utilizes 2D bounding boxes from a pre-trained 2D detector [68] to build pseudo-3D label for object localization. [58] leverages various 2D foundation models to enhance the performance of 3D open-vocabulary detection. More recently, OV-Uni3DETR [54] proposes a multi-modal open-vocabulary 3D detector that accommodates both point clouds and images as the input. In contrast, our work focuses on the monocular 3D detection task that only requires RGB images as input and does not assume the availability of point cloud data at training or inference phases.

Monocular 3D Object Detection refers to the task of identifying and localizing objects within a scene using 3D bounding boxes derived from single-view images. Early research in this domain primarily targeted either outdoor [10, 11, 22, 52, 53, 64, 66, 67] or indoor [13, 23, 37, 46] environments, focusing on specialized applications such as autonomous driving in urban areas and room layout estimation. The release of the extensive Omni3D dataset enabled Cube R-CNN [5] to pioneer unified monocular 3D object detection, allowing detectors to be effectively applied across multiple scene types and significantly enhancing their generalization capabilities. Following this, UniMODE [30] introduced the first successful BEV-based monocular 3D object detector capable of operating in both indoor and outdoor settings, demonstrating increased versa-

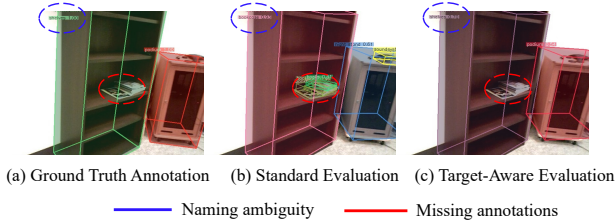


Figure 3. **Target-Aware Evaluation.** (a) **Naming ambiguity** and **missing annotations** are common in the benchmarks. In this example, the 3D annotations are missing for “books”; the “shelves” share high similarity with “bookcases”. (b) This induces inaccurate performance assessment of open-vocabulary 3D detection under the standard evaluation. (c) Our target-aware evaluation effectively resolves this issue by prompting the categories presented in the annotations.

tivity in diverse environments. However, most of these approaches suffer from limited generalizability, and even advanced models like Cube R-CNN [5] and UniMODE [30] are constrained by a closed vocabulary, restricting their ability to recognize or detect object classes that were not included during training. To address this limitation, our work focuses on exploring the potential of monocular open-vocabulary 3D detection.

3. Open Vocabulary Monocular 3D Detection

3.1. Task Definition

Formally, given an input image $I \in \mathbb{R}^{H \times W \times 3}$ and a text prompt $T = [c_1, c_2, \dots, c_M]$ consisting of all possible category names from an open vocabulary \mathcal{C} , the objective of this task is to predict a set of objects $\{(c_i, B_i)\}_{i=1}^N$, where:

- $c_i \in T$ is the predicted category label for object i .
- B_i is the parameters of the 3D bounding box in the camera coordinate system, defined in metric space.

The vocabulary \mathcal{C} is divided into two subsets: *base categories* $\mathcal{C}_{\text{base}}$, which are seen during training, and *novel categories* $\mathcal{C}_{\text{novel}}$, which are unseen during training and only evaluated during inference. The model is trained to predict the 3D bounding boxes for objects in $\mathcal{C}_{\text{base}}$ and generalize to $\mathcal{C}_{\text{novel}}$ without additional fine-tuning.

3.2. Evaluation Metrics

Standard Metrics. Mean Average Precision ($\text{AP}_{3\text{D}}$) based on Intersection over Union (IoU) is the widely used standard metric for closed-vocabulary 3D object detection tasks [5, 30]. However, directly applying traditional evaluation protocols to OVMONO3D presents challenges due to common issues in 3D dataset annotations:

- *Missing annotations:* Comprehensive 3D annotation is often impractical due to high costs. Fig. 3a illustrates an example of this issue from Omni3D [5].

- *Naming ambiguity:* Objects may be labeled with different conventions or policies during annotation (e.g., table vs. desk). Standard open-vocabulary 2D detection methods typically prompt 2D detectors with exhaustive lists of possible categories, which can lead to correct predictions with class names that do not align with the dataset annotations, especially for vaguely defined or overlapping categories, as shown in Fig. 3b.

Target-Aware Metrics. To address these issues, we propose a customized evaluation approach that considers only the categories with ground-truth labeled instances in each image. Specifically, instead of providing the 2D detector with an exhaustive list of possible categories, we only prompt it with category names that exist in the annotations for each image. Since human annotators typically label all instances of the same category within a single image, categories with ground-truth annotations are likely to be fully annotated.

Our target-aware evaluation prevents the negative effects of missing annotations on metrics by focusing only on categories present in the ground-truth annotations. It also excludes irrelevant categories that could distract the 2D detector. As shown in Fig. 3c, by concentrating on relevant categories, this approach mitigates the impact of missing annotations and reduces category ambiguity, enabling a more accurate assessment of the model’s 3D detection capabilities.

4. Methodology

Our approach builds on two state-of-the-art frameworks: Cube R-CNN [5] for monocular 3D detection and Grounding DINO [32] for open-vocabulary (OV) 2D detection. In this section, we first provide a brief overview of these two frameworks (Sec. 4.1); we then introduce our two proposed methods for addressing OVMONO3D (Sec. 4.2 - 4.3).

4.1. Preliminaries

Cube R-CNN [5] is a state-of-the-art monocular 3D detection model, which is trained from a large-scale 3D dataset (i.e., Omni3D). It extends Faster R-CNN [44] with a 3D cube head. Using 2D region proposals as input, the cube head employs ROI poolers to extract local image features and then predicts 3D bounding boxes with MLPs. Each 3D bounding box B_i is defined by its geometric parameters:

- *Position:* $t_i = [x_i, y_i, z_i]^T \in \mathbb{R}^3$, the 3D coordinates of the object’s center in metric space.
- *Dimensions:* $d_i = [w_i, h_i, l_i]^T \in \mathbb{R}^3$, representing width, height, and length in meters.
- *Orientation:* Represented by a continuous 6D allocentric rotation $r_i \in \mathbb{R}^6$ [69].

The training objective of Cube R-CNN is defined as:

$$\mathcal{L} = \mathcal{L}_{2D} + \sqrt{2} \exp(-\mu) \mathcal{L}_{3D} + \mu, \quad (1)$$

where \mathcal{L}_{2D} includes the classification and bounding box regression losses from the 2D detection head [44], \mathcal{L}_{3D} is the loss from the 3D cube head, and μ denotes the uncertainty score. The 3D loss \mathcal{L}_{3D} consists of disentangled losses for each 3D attribute [50]:

$$\mathcal{L}_{3D} = \sum_a \mathcal{L}_{3D}^{(a)} + \mathcal{L}_{3D}^{\text{all}}, \quad (2)$$

where $a \in \{(x_{2D}, y_{2D}), z, (w, h, l), r\}$ represents variable groups for the 2D center shift, depth, dimensions, and rotation. Each disentangled loss $\mathcal{L}_{3D}^{(a)}$ isolates the error of a specific group by substituting other predicted variables with ground-truth values when constructing the predicted 3D bounding box B_{3D} . The holistic loss $\mathcal{L}_{3D}^{\text{all}}$ compares the predicted 3D bounding box with the ground truth using the Chamfer Loss:

$$\mathcal{L}_{3D}^{\text{all}} = \ell_{\text{Chamfer}}(B_{3D}, B_{3D}^{\text{gt}}). \quad (3)$$

Grounding DINO [32] is a leading framework for OV 2D detection, which combines the Transformer-based DINO detector [59] with grounded pretraining. We adopt a pre-trained Grounding DINO as our default OV 2D detection model due to its superior performance and strong zero-shot generalization capabilities. An ablation study on the effect of different base 2D detection models on our approach is provided in Sec. 5.

4.2. OVMONO3D-GEO: Geometric 2D Unprojection

To perform OV 3D detection from a single image, a simple approach is to unproject 2D detections into 3D using geometric principles. Specifically, given an input image I , a text prompt T , and 2D bounding boxes with category labels $\{(b_i, c_i)\}_{i=1}^N$ predicted by an OV 2D detector [32], the method proceeds as follows.

For each detected object (b_i, c_i) , an instance segmentation mask S_i is obtained using a segmentation model (e.g., SAM [26]), and a metric depth estimation model (e.g., Depth Pro [4]) generates the depth map $D \in \mathbb{R}^{H \times W}$. Pixels within S_i are unprojected into 3D space using the camera intrinsic matrix $K \in \mathbb{R}^{3 \times 3}$ to form a point cloud P_i . Here, u and v denote the pixel coordinates in the image, and each 3D point $p = [x, y, z]^T \in P_i$ is computed as:

$$p = D(u, v) \cdot K^{-1} \begin{bmatrix} u & v & 1 \end{bmatrix}^T.$$

To estimate the 3D bounding box parameters $B_i = (t_i, d_i, r_i)$, Principal Component Analysis (PCA) determines the orientation r_i , dimensions d_i , and centroid t_i of P_i . DBSCAN [14] removes outliers, improving robustness against noisy masks and depth predictions.

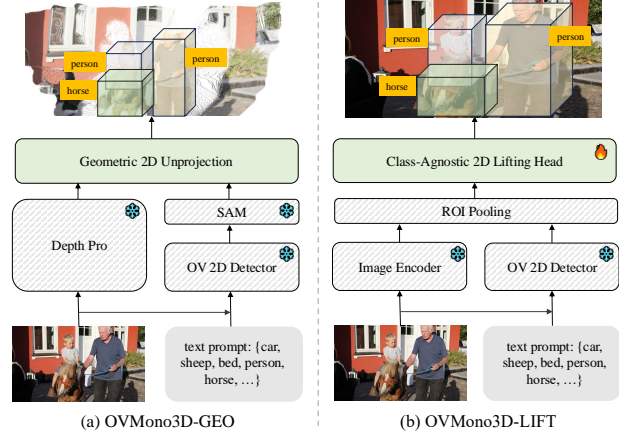


Figure 4. **Proposed Methods.** (a) OVMONO3D-GEO is a training-free method that predicts 3D detections from 2D via geometric unprojection. It exploits off-the-shelf depth estimation (i.e. Depth Pro [4]), segmentation (i.e. SAM [26]), and OV 2D detector [32]. (b) OVMONO3D-LIFT is a learning-based approach that trains a class-agnostic neural network to lift 2D detections to 3D. Both approaches disentangle the recognition and location in 2D from the estimation of 3D bounding boxes.

This geometric approach reconstructs 3D bounding boxes from 2D detections without relying on learned 3D attributes, providing a non-learning-based benchmark for evaluating OV 3D object detection models. Its accuracy depends on the quality of D and S_i , and is sensitive to occlusions, which may cause incomplete point clouds and inaccuracies in the reconstructed bounding boxes.

4.3. OVMONO3D-LIFT: Class-Agnostic 2D Lifting

Given the limitations of geometric-based methods, we propose leveraging monocular 3D annotations to build data-driven models. As depicted in Fig. 2, 3D annotations are far fewer than 2D annotations. To address this, we utilize off-the-shelf 2D data-driven priors to enhance 3D performance. Specifically, we introduce OVMONO3D-LIFT, which decouples OV monocular 3D detection into two stages: (1) recognizing and localizing objects in 2D using off-the-shelf OV 2D detectors, and (2) class-agnostically lifting the 2D bounding boxes to 3D cuboids.

Given an image I , a text prompt T , and 2D bounding boxes with category labels $\{(b_i, c_i)\}_{i=1}^N$ predicted by an OV 2D detector [32], OVMONO3D-LIFT employs a pretrained Vision Transformer (ViT-B/14) backbone to extract an image feature map $F \in \mathbb{R}^{\frac{H}{14} \times \frac{W}{14} \times C}$, where C is the feature dimension. A Simple Feature Pyramid (SFP) [29] module generates three feature maps with scaling factors 0.5, 1, and 2, forming a multi-scale hierarchical pyramid. The predicted 2D bounding boxes are used as regions of interest for ROI pooling, extracting local object features of size 7×7 . These features are fed into a cube head, as described

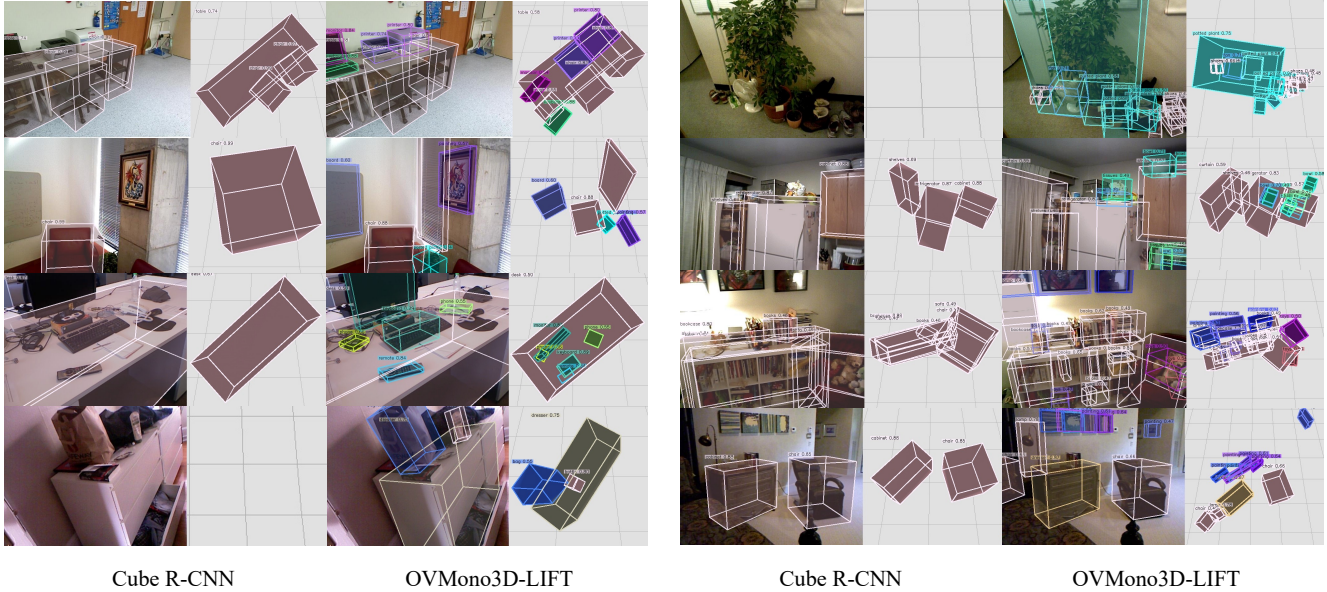


Figure 5. **Qualitative Visualizations on the Omni3D Test Set.** For each example, we present the predictions of Cube R-CNN and OVMONO3D-LIFT, displaying both the 3D predictions overlaid on the image and a top-down view with a base grid of $1\text{ m} \times 1\text{ m}$ tiles. Base categories are depicted with brown cubes, while novel categories are represented in other colors. See Appendix B for more visualizations.

in Sec. 4.1, to predict 3D attributes. Unlike [5], our attribute prediction head is *class-agnostic*, while their method employs class-specific layers and per-class average size statistics, which limit generalization to open vocabularies. The training objective is identical to Cube R-CNN, as described in Sec. 4.1.

Baseline Methods. An alternative data-driven approach is to directly extend OV 2D detectors to 3D. Specifically, we use the output features from the final decoder layer of Grounding DINO [32] as object representations, which are then processed by an MLP to predict 3D attributes. While straightforward, this method does not leverage pretrained image encoders (e.g. DINOv2 [38]). Therefore, we use it as a baseline for comparison.

We evaluate two variants of this method: (1) **G-DINO-3D (FZ)**, where only the additional MLP is trainable and other parameters are frozen, and (2) **G-DINO-3D (FT)**, where we fine-tune all network parameters. Both variants are initialized with the pretrained weights of Grounding DINO and follow the same training objective as Cube R-CNN, as outlined in Sec. 4.1.

5. Experiments

5.1. Experimental Setup

Datasets. The experiments are conducted using the Omni3D [5] dataset, the largest publicly available dataset for monocular 3D object detection across both indoor and

outdoor scenes. Omni3D is repurposed and combined from six established sources including SUN RGB-D [51], ARK-itScenes [2], Objectron [1], Hypersim [45], nuScenes [6], and KITTI [15]. It comprises a substantial 234k images, 3 million labeled 3D bounding boxes, and covers 98 distinct object categories.

During training, we use the 50 categories Cube R-CNN [5] trained on as the base categories for model training. For evaluation, we select 22 categories from the remaining classes as novel categories. These categories are chosen based on two criteria: the number of test instances and the precision of category naming. To facilitate a detailed assessment of zero-shot generalization capabilities, we further divide these categories into *easy* and *hard* subsets according to object visibility. The easy categories include *board*, *printer*, *painting*, *microwave*, *tray*, *podium*, *cart*, and *tram*, while the remaining categories constitute the hard subset.

Evaluations. We report a mean AP_{3D} across all 50 base categories and 22 novel categories in Omni3D and over a range of IoU3D thresholds $\tau \in [0.05, 0.10, \dots, 0.50]$. Unless explicitly stated otherwise, all the evaluations are under our target-aware evaluation protocols (Sec. 3.2).

Besides the standard IoU metrics, we also report the Normalized Hungarian Distance (NHD) [3] which provides a more precise evaluation. NHD computes the normalized distance between predicted and ground-truth cube corners using the Hungarian matching algorithm. NHD is computed

| Methods | AP _{2D} ↑ | AP _{3D} ↑ | AP _{3D} ¹⁵ ↑ | AP _{3D} ²⁵ ↑ | AP _{3D} ⁵⁰ ↑ | AP _{3D} ^{easy} ↑ | AP _{3D} ^{hard} ↑ |
|----------------|--------------------|--------------------|----------------------------------|----------------------------------|----------------------------------|------------------------------------|------------------------------------|
| G-DINO-3D (FT) | 6.77 | 4.43 | 6.21 | 4.92 | 1.12 | 4.77 | 4.24 |
| G-DINO-3D (FZ) | 19.22 | 3.54 | 5.74 | 2.71 | 0.07 | 4.59 | 2.96 |
| OVMONO3D-GEO | 18.72 | 9.03 | 14.88 | 7.60 | 0.43 | 12.55 | 7.01 |
| OVMONO3D-LIFT | 21.59 | 16.05 | 24.27 | 14.97 | 2.40 | 20.58 | 13.47 |

Table 1. **Performance of OVMONO3D-LIFT and Baselines on Novel Categories.** We report AP_{2D} and AP_{3D}, followed by AP_{3D} at IoU thresholds of 0.15, 0.25, and 0.50, for both easy and hard objects. The best results for each metric are highlighted in **bold**. G-DINO-3D denotes the extending Grounding DINO to 3D baseline described in Sec. 4.3. FT refers to the fine-tuned model, FZ refers to the 2D detection weights being frozen. See Appendix A for per-category performance.

| | AP _{2D} ↑ | AP _{3D} ↑ | AP _{3D} ¹⁵ ↑ | AP _{3D} ²⁵ ↑ | AP _{3D} ⁵⁰ ↑ |
|-----------------------|--------------------|--------------------|----------------------------------|----------------------------------|----------------------------------|
| Cube R-CNN [5] | 32.31 | 26.78 | 35.71 | 28.72 | 10.48 |
| OVMONO3D-LIFT | | | | | |
| + Grounding DINO [32] | 21.96 | 24.77 | 33.23 | 26.33 | 9.38 |
| + Cube R-CNN [5] | 32.45 | 26.44 | 35.30 | 28.40 | 10.26 |
| + Ground Truth | 100 | 29.07 | 39.74 | 30.38 | 10.39 |

Table 2. **Performance of OVMONO3D-LIFT on Base Categories.** We compare our model with Cube R-CNN on the Omni3D test set. “+” indicates the different 2D box inputs used, including predictions from Grounding DINO, Cube R-CNN, and ground truth 2D boxes.

for predictions that have a high IoU with the ground-truth 2D bounding boxes. Therefore, NHD values for different methods with varying 2D inputs are not directly comparable. To disentangle the error contributions of different predicted attributes to the overall 3D bounding box prediction, we report disentangled NHD for the position (XY), depth, dimensions, and pose. For each attribute, we compute the NHD of a disentangled 3D bounding box that uses the predicted value for that attribute while setting the other attributes to their ground-truth values, comparing it with the ground-truth cube.

Implementation Details. Our implementation is based on Pytorch3D [43] and Detectron2 [56]. We utilize DINOv2 [38] as the image feature encoder, freezing all parameters during training. All experiments are conducted on four NVIDIA A100 GPUs. The models are trained for 116k steps with a batch size of 64. We employ SGD with an initial learning rate of 0.012, which decays by a factor of 10 at 60% and 80% of the training duration. During training, image augmentations including random horizontal flipping and resizing are applied.

5.2. Model Performance

Fig. 5 shows qualitative results on the Omni3D test set. In comparison with Cube R-CNN [5], OVMONO3D-LIFT detects not only objects of base categories, but also novel categories that are unseen at the training time.

Novel Category Performance. Tab. 1 shows that OVMONO3D-LIFT outperforms the baseline methods on novel categories by a large margin. OVMONO3D-GEO demonstrates lower performance due to its sensitivity to occlusions and inaccuracies in metric depth map estimation. G-DINO-3D (FZ) freezes the 2D detection parameters, resulting in object features that are not well-suited for 3D detection. Conversely, G-DINO-3D (FT) fine-tunes the model, degrading its original OV detection capabilities, since monocular 3D detection lacks the extensive detection and grounding annotations available in 2D. Therefore, these approaches are suboptimal. In contrast, OVMONO3D-LIFT effectively leverages 2D data-driven priors, including OV 2D detectors and self-supervised 2D features, by decoupling the OVMONO3D task into OV 2D detection and 2D-to-3D unprojection. This approach mitigates issues related to low-quality and scarce annotations in 3D, leading to superior performance.

Base Category Performance. Tab. 2 compares OVMONO3D-LIFT with Cube R-CNN on base categories using different 2D bounding box inputs. When using the OV 2D detector’s predictions as input, OVMONO3D-LIFT shows lower performance due to the OV 2D detector’s lower zero-shot performance on the Omni3D test set. In contrast, when using Cube R-CNN’s 2D predictions, OVMONO3D-LIFT achieves comparable performance to Cube R-CNN. Notably, Cube R-CNN utilizes per-category priors for object dimensions and depth, highlighting the superior performance of OVMONO3D-LIFT without relying on such priors. Additionally, we provide results with ground-truth 2D inputs as a reference.

5.3. Analysis

Evaluation Protocol. Tab. 3 shows that our target-aware evaluation leads to increased metrics on both base and novel category settings. Even for the original Cube R-CNN, our method demonstrates improvements in both AP_{2D} and AP_{3D}, indicating its effectiveness in eliminating the adverse effects of missing annotations. On novel categories, our target-aware evaluation shows considerable metric value gains. This improvement is particularly important because

| Models | Original Evaluation | | | | Target-Aware Evaluation | | | |
|-----------------------|---------------------|-------------------|-------------------|-------------------|-------------------------|-------------------------|-------------------------|-------------------------|
| | \tilde{AP}_{2D} | \tilde{AP}_{3D} | \tilde{AR}_{2D} | \tilde{AR}_{3D} | AP_{2D} | AP_{3D} | AR_{2D} | AR_{3D} |
| Cube R-CNN (Base) | 27.65 | 23.68 | 42.35 | 37.56 | 32.31 ^{+4.66} | 26.78 ^{+3.10} | 42.35 ^{+0.00} | 37.56 ^{+0.00} |
| OVMONO3D-LIFT (Base) | 12.27 | 17.22 | 27.19 | 33.45 | 21.96 ^{+9.69} | 24.77 ^{+7.55} | 40.13 ^{+12.94} | 47.28 ^{+13.83} |
| OVMONO3D-LIFT (Novel) | 7.01 | 4.22 | 17.86 | 15.58 | 21.59 ^{+14.58} | 16.05 ^{+11.83} | 37.88 ^{+20.02} | 36.85 ^{+21.27} |

Table 3. **Comparison of Original and Target-Aware Evaluation.** Mean Average Recall (AR) for 2D and 3D under the same IoU thresholds as AP is also reported. Metrics marked with a tilde denote results from the original evaluation protocol (Section 3.2). Improvements from target-aware evaluation over the original are highlighted in purple.

| Methods | NHD | XY | Depth | Size | Pose |
|---------------|------|------|-------|------|------|
| OVMONO3D-GEO | 5.47 | 2.23 | 4.30 | 2.34 | 2.04 |
| OVMONO3D-LIFT | 5.72 | 2.28 | 4.73 | 1.05 | 0.55 |

Table 4. **Disentangled Metrics.** We report the overall and disentangled NHD for different attribute predictions. Since NHD is only computed on high-IoU predictions — which usually vary across different models — comparisons are valid only within each model. Lower values indicate better performance.

| 2D Box Input | $AP_{2D}\uparrow$ | $AP_{3D}\uparrow$ | $AP_{3D}^{15}\uparrow$ | $AP_{3D}^{25}\uparrow$ | $AP_{3D}^{50}\uparrow$ |
|----------------|-------------------|-------------------|------------------------|------------------------|------------------------|
| Ground Truth | 100 | 17.21 | 25.71 | 16.30 | 2.79 |
| YOLO-World | 20.14 | 12.82 | 20.25 | 11.91 | 1.63 |
| Grounding DINO | 21.59 | 16.05 | 24.27 | 14.97 | 2.40 |

Table 5. **Ablation on 2D Bounding Box Input.** Evaluation of open-vocabulary 2D detectors and their impact on 2D and 3D detection performance for novel categories.

novel categories are often infrequent and smaller in size, making them harder for the model to detect when prompted with an extensive list of possible categories.

Disentangled Metrics. Tab. 4 exhibits the overall and disentangled NHD for different attribute predictions. For these two methods, object depth prediction consistently contributes the most error to the overall prediction. This indicates that object depth estimation is the primary bottleneck of our task. Furthermore, the size and pose predictions in OVMONO3D-GEO exhibit larger errors, indicating that geometry-based methods are not effective for these predictions. This underscores the necessity of developing learning-based methods.

2D Bounding Box Input. Tab. 5 evaluates the impact of 2D detectors on both 2D and 3D detection performance for novel categories. We test two state-of-the-art 2D detectors: YOLO-World [12] and Grounding DINO [32], alongside ground-truth 2D bounding boxes as reference. Grounding DINO consistently outperforms YOLO-World across all evaluation metrics. Notably, the 3D lifting results from Grounding DINO’s zero-shot 2D detection are only 1% lower than the performance with ground-truth 2D input in

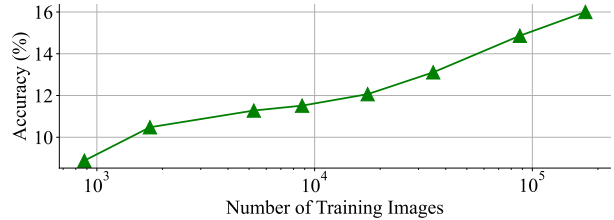


Figure 6. The performance of OVMONO3D-LIFT as a function of training data amount. We report the AP_{3D} (%) on novel categories as the evaluation metric.

terms of AP_{3D} , demonstrating that Grounding DINO is a preferable off-the-shelf 2D detector for OVMONO3D.

Pre-trained Backbone Selection. Tab. 6 shows the impact of pretrained feature extractors on 3D detection performance for novel categories. DINOv2 achieves the best performance across all evaluation metrics. This result underscores the effectiveness of DINOv2’s representations for the 3D detection task. Our findings align with recent studies that highlight DINOv2’s strong zero-shot capabilities in understanding depth, multi-view correspondences, and relative pose [17, 27, 62], demonstrating that DINOv2’s features are highly suitable for this task.

Training Data Scaling Law. Fig. 6 reports our model’s AP_{3D} score as a function of the training data size. This underscores the critical importance of dataset size in open vocabulary monocular 3D object detection tasks and suggests that our model may achieve even better performance with more extensive training data.

Do synthetic data help? Tab. 7 presents the effect of synthetic data on the performance of OVMONO3D-LIFT. When synthetic data is incorporated alongside real data, a modest yet meaningful increase of 1 AP_{3D} point is observed in detecting objects from seen categories, while performance on novel categories remains largely unchanged. These findings suggest that, while synthetic data can enhance model performance in closed-vocabulary 3D object detection tasks, its benefits are minimal for detecting unseen objects, thereby limiting its usefulness in open-vocabulary 3D object detection scenarios.

| Feature Extractor | Arch. | Supervision | Dataset | AP _{3D} ↑ | AP _{3D} ¹⁵ ↑ | AP _{3D} ²⁵ ↑ | AP _{3D} ⁵⁰ ↑ |
|-------------------|----------|-------------|------------|--------------------|----------------------------------|----------------------------------|----------------------------------|
| MAE [21] | ViT-B/16 | SSL | ImageNet1k | 7.72 | 11.95 | 6.43 | 0.80 |
| CLIP [41] | ViT-B/16 | VLM | WIT-400M | 9.02 | 14.19 | 8.44 | 0.50 |
| MiDas [42] | ViT-L/16 | Depth | MIX-6 | 10.65 | 17.42 | 9.87 | 0.69 |
| DINOv2 [38] | ViT-B/14 | SSL | LVD-142M | 16.05 | 24.27 | 14.97 | 2.40 |

Table 6. **Ablation Study on Feature Extractors for OVMONO3D-LIFT in 3D Detection on Novel Categories.** We report AP_{3D} for various feature extractors with frozen parameters during training.

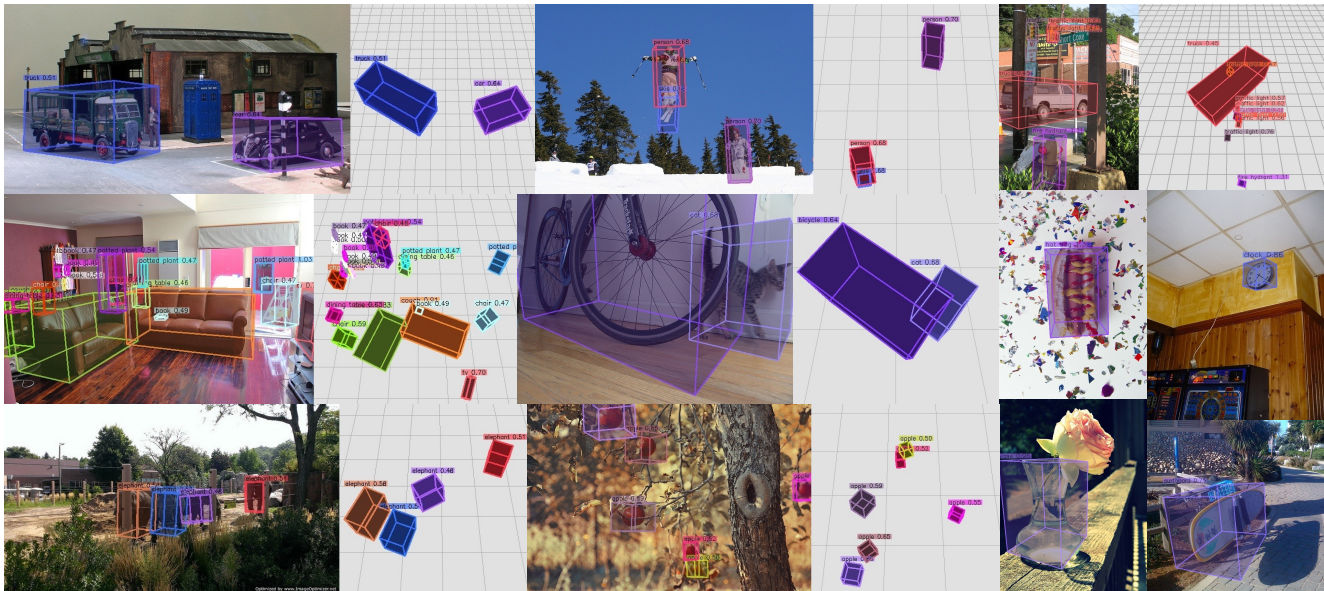


Figure 7. **OVMONO3D-LIFT on In-the-Wild COCO Images.** We display 3D predictions overlaid on the images and the top-down views with a base grid of 1 m × 1 m tiles. For single-object images, only front-views are displayed. Results are shown for both base and novel categories, demonstrating that OVMONO3D-LIFT exhibits zero-shot generalization capability on real-world images.

| Data | #Images | AP _{3D} ^{Base} | AP _{3D} ^{Novel} |
|----------------|---------|----------------------------------|-----------------------------------|
| Synthetic | 55k | 7.14 | 7.33 |
| Real | 120k | 23.78 | 16.20 |
| Synthetic+Real | 175k | 24.77 | 16.05 |

Table 7. **Ablation on Synthetic Data.** Synthetic data boosts the performance of OVMONO3D-LIFT on base categories but offers little benefit for novel objects.

5.4. Zero-Shot Generalization Performance

Fig. 7 presents OVMONO3D-LIFT prediction on in-the-wild images from COCO [31]. We visualize with intrinsics of $f = 2 \cdot H$, $p_x = \frac{1}{2}W$, $p_y = \frac{1}{2}H$, where $H \times W$ is the input image resolution. The results show 2D projections of our predictions are well-aligned with the objects, and their top-down views closely match the visual scene layout. Even on completely out-of-distribution categories such as elephant and apple, our method produces promising results. This suggests that our model demonstrates zero-shot generalization ability on real-world images.

6. Discussion

We investigate OVMONO3D, an under-explored task of recognizing and localizing objects from any categories in 3D using a single image. We identify unique challenges, notably data scarcity and limitations of standard evaluation metrics. We propose simple yet effective approaches, including geometry-based OVMONO3D-GEO and learning-based OVMONO3D-LIFT — both decouple 2D detection from 3D bounding box prediction. Such design enables the full utilization of off-the-shelf open-vocabulary 2D detectors pre-trained on large-scale datasets. Our analysis pinpoints the key components in the framework, including pre-trained image encoder, base 2D detectors, and the impact of dataset scaling. We further demonstrate the zero-shot generalizability of our approach on in-the-wild images. Our findings suggest that dataset scale and accurate depth perception remain the major bottlenecks in this task. One promising direction may be to develop unsupervised learning that harness the abundance of unlabeled images. We hope this work inspires future research toward advancing this task.

Acknowledgement. The authors acknowledge Research Computing at The University of Virginia for providing computational resources and technical support that have contributed to the results reported within this publication.

References

- [1] Adel Ahmadyan, Liangkai Zhang, Artsiom Ablavatski, Jianing Wei, and Matthias Grundmann. Objectron: A large scale dataset of object-centric videos in the wild with pose annotations. In *CVPR*, 2021. 5
- [2] Gilad Baruch, Zhuoyuan Chen, Afshin Dehghan, Yuri Feigin, Peter Fu, Thomas Gebauer, Daniel Kurz, Tal Dimry, Brandon Joffe, Arik Schwartz, et al. Arkitscenes: A diverse real-world dataset for 3d indoor scene understanding using mobile rgb-d data. In *NeurIPS*, 2021. 5
- [3] Wenjing Bian, Zirui Wang, and Andrea Vedaldi. Catfree3d: Category-agnostic 3d object detection with diffusion. *arXiv preprint arXiv:2408.12747*, 2024. 5
- [4] Aleksei Bochkovskii, Amaël Delaunoy, Hugo Germain, Marcel Santos, Yichao Zhou, Stephan R Richter, and Vladlen Koltun. Depth pro: Sharp monocular metric depth in less than a second. *arXiv preprint arXiv:2410.02073*, 2024. 4
- [5] Garrick Brazil, Abhinav Kumar, Julian Straub, Nikhila Ravi, Justin Johnson, and Georgia Gkioxari. Omni3d: A large benchmark and model for 3d object detection in the wild. In *CVPR*, 2023. 1, 2, 3, 5, 6
- [6] Holger Caesar, Varun Bankiti, Alex H Lang, Sourabh Vora, Venice Erin Liong, Qiang Xu, Anush Krishnan, Yu Pan, Giancarlo Baldan, and Oscar Beijbom. nuscenes: A multi-modal dataset for autonomous driving. In *CVPR*, 2020. 5
- [7] Yang Cao, Zeng Yihan, Hang Xu, and Dan Xu. Coda: Collaborative novel box discovery and cross-modal alignment for open-vocabulary 3d object detection. *NeurIPS*, 2024. 2
- [8] Yang Cao, Yihan Zeng, Hang Xu, and Dan Xu. Collaborative novel object discovery and box-guided cross-modal alignment for open-vocabulary 3d object detection. *arXiv preprint arXiv:2406.00830*, 2024. 2
- [9] Nicolas Carion, Francisco Massa, Gabriel Synnaeve, Nicolas Usunier, Alexander Kirillov, and Sergey Zagoruyko. End-to-end object detection with transformers. In *European conference on computer vision*, pages 213–229. Springer, 2020. 1
- [10] Hansheng Chen, Yuyao Huang, Wei Tian, Zhong Gao, and Lu Xiong. Monorun: Monocular 3d object detection by reconstruction and uncertainty propagation, 2021. 2
- [11] Xiaozhi Chen, Kaustav Kundu, Ziyu Zhang, Huimin Ma, Sanja Fidler, and Raquel Urtasun. Monocular 3d object detection for autonomous driving. In *CVPR*, 2016. 2
- [12] Tianheng Cheng, Lin Song, Yixiao Ge, Wenyu Liu, Xingang Wang, and Ying Shan. Yolo-world: Real-time open-vocabulary object detection. In *CVPR*, 2024. 1, 2, 7
- [13] Saumitro Dasgupta, Kuan Fang, Kevin Chen, and Silvio Savarese. Delay: Robust spatial layout estimation for cluttered indoor scenes. In *CVPR*, 2016. 2
- [14] Martin Ester, Hans-Peter Kriegel, Jörg Sander, Xiaowei Xu, et al. A density-based algorithm for discovering clusters in large spatial databases with noise. In *kdd*, pages 226–231, 1996. 4
- [15] Andreas Geiger, Philip Lenz, and Raquel Urtasun. Are we ready for autonomous driving? the kitti vision benchmark suite. In *CVPR*, 2012. 5, 2
- [16] R Girshick. Fast r-cnn. *arXiv preprint arXiv:1504.08083*, 2015. 1
- [17] Walter Goodwin, Sagar Vaze, Ioannis Havoutis, and Ingmar Posner. Zero-shot category-level object pose estimation. In *ECCV*, 2022. 7
- [18] Xiuye Gu, Tsung-Yi Lin, Weicheng Kuo, and Yin Cui. Open-vocabulary object detection via vision and language knowledge distillation. *arXiv preprint arXiv:2104.13921*, 2021. 2
- [19] Agrim Gupta, Piotr Dollar, and Ross Girshick. Lvis: A dataset for large vocabulary instance segmentation. In *Proceedings of the IEEE/CVF conference on computer vision and pattern recognition*, pages 5356–5364, 2019. 1
- [20] Kaiming He, Georgia Gkioxari, Piotr Dollár, and Ross Girshick. Mask r-cnn. In *Proceedings of the IEEE international conference on computer vision*, pages 2961–2969, 2017. 1
- [21] Kaiming He, Xinlei Chen, Saining Xie, Yanghao Li, Piotr Dollár, and Ross Girshick. Masked autoencoders are scalable vision learners. In *CVPR*, 2022. 8
- [22] Kuan-Chih Huang, Tsung-Han Wu, Hung-Ting Su, and Winston H Hsu. Monodr: Monocular 3d object detection with depth-aware transformer. In *CVPR*, pages 4012–4021, 2022. 2
- [23] Siyuan Huang, Siyuan Qi, Yinxue Xiao, Yixin Zhu, Ying Nian Wu, and Song-Chun Zhu. Cooperative holistic scene understanding: Unifying 3d object, layout, and camera pose estimation, 2019. 2
- [24] Chao Jia, Yinfei Yang, Ye Xia, Yi-Ting Chen, Zarana Parekh, Hieu Pham, Quoc Le, Yun-Hsuan Sung, Zhen Li, and Tom Duerig. Scaling up visual and vision-language representation learning with noisy text supervision. In *ICML*, pages 4904–4916, 2021. 2
- [25] Aishwarya Kamath, Mannat Singh, Yann LeCun, Gabriel Synnaeve, Ishan Misra, and Nicolas Carion. Mdet: Modulated detection for end-to-end multi-modal understanding. In *ICCV*, 2021. 2
- [26] Alexander Kirillov, Eric Mintun, Nikhila Ravi, Hanzi Mao, Chloe Rolland, Laura Gustafson, Tete Xiao, Spencer Whitehead, Alexander C Berg, Wan-Yen Lo, et al. Segment anything. In *ICCV*, 2023. 4
- [27] Akshay Krishnan, Abhijit Kundu, Kevis-Kokitsi Maninis, James Hays, and Matthew Brown. Omninocs: A unified nocs dataset and model for 3d lifting of 2d objects. In *ECCV*, 2025. 7
- [28] Liunian Harold Li, Pengchuan Zhang, Haotian Zhang, Jianwei Yang, Chunyuan Li, Yiwu Zhong, Lijuan Wang, Lu Yuan, Lei Zhang, Jenq-Neng Hwang, et al. Grounded language-image pre-training. In *CVPR*, 2022. 2
- [29] Yanghao Li, Hanzi Mao, Ross Girshick, and Kaiming He. Exploring plain vision transformer backbones for object detection. In *ECCV*, 2022. 4

- [30] Zhuoling Li, Xiaogang Xu, SerNam Lim, and Hengshuang Zhao. Towards unified 3d object detection via algorithm and data unification, 2024. **2, 3**
- [31] Tsung-Yi Lin, Michael Maire, Serge Belongie, James Hays, Pietro Perona, Deva Ramanan, Piotr Dollár, and C Lawrence Zitnick. Microsoft coco: Common objects in context. In *ECCV*, 2014. **1, 8, 3, 4, 5**
- [32] Shilong Liu, Zhaoyang Zeng, Tianhe Ren, Feng Li, Hao Zhang, Jie Yang, Qing Jiang, Chunyuan Li, Jianwei Yang, Hang Su, et al. Grounding dino: Marrying dino with grounded pre-training for open-set object detection. *arXiv preprint arXiv:2303.05499*, 2023. **1, 2, 3, 4, 5, 6, 7**
- [33] Yuheng Lu, Chenfeng Xu, Xiaobao Wei, Xiaodong Xie, Masayoshi Tomizuka, Kurt Keutzer, and Shanghang Zhang. Open-vocabulary 3d detection via image-level class and de-biased cross-modal contrastive learning. *arXiv preprint arXiv:2207.01987*, 2022. **2**
- [34] Yuheng Lu, Chenfeng Xu, Xiaobao Wei, Xiaodong Xie, Masayoshi Tomizuka, Kurt Keutzer, and Shanghang Zhang. Open-vocabulary point-cloud object detection without 3d annotation. In *CVPR*, 2023. **2**
- [35] Zongyang Ma, Guan Luo, Jin Gao, Liang Li, Yuxin Chen, Shaoru Wang, Congxuan Zhang, and Weiming Hu. Open-vocabulary one-stage detection with hierarchical visual-language knowledge distillation. In *CVPR*, 2022. **2**
- [36] Matthias Minderer, Alexey Gritsenko, Austin Stone, Maxim Neumann, Dirk Weissenborn, Alexey Dosovitskiy, Aravindh Mahendran, Anurag Arnab, Mostafa Dehghani, Zhuoran Shen, et al. Simple open-vocabulary object detection. In *ECCV*, 2022. **2**
- [37] Yinyu Nie, Xiaoguang Han, Shihui Guo, Yujian Zheng, Jian Chang, and Jian Jun Zhang. Total3dunderstanding: Joint layout, object pose and mesh reconstruction for indoor scenes from a single image, 2020. **1, 2**
- [38] Maxime Oquab, Timothée Darcet, Théo Moutakanni, Huy Vo, Marc Szafraniec, Vasil Khalidov, Pierre Fernandez, Daniel Haziza, Francisco Massa, Alaaeldin El-Nouby, et al. Dinov2: Learning robust visual features without supervision. *arXiv preprint arXiv:2304.07193*, 2023. **5, 6, 8**
- [39] Vicente Ordonez, Girish Kulkarni, and Tamara Berg. Im2text: Describing images using 1 million captioned photographs. *NeurIPS*, 2011. **2**
- [40] Xingyu Peng, Yan Bai, Chen Gao, Lirong Yang, Fei Xia, Beipeng Mu, Xiaofei Wang, and Si Liu. Global-local collaborative inference with llm for lidar-based open-vocabulary detection. In *ECCV*. Springer, 2025. **2**
- [41] Alec Radford, Jong Wook Kim, Chris Hallacy, Aditya Ramesh, Gabriel Goh, Sandhini Agarwal, Girish Sastry, Amanda Askell, Pamela Mishkin, Jack Clark, et al. Learning transferable visual models from natural language supervision. In *ICML*, 2021. **2, 8**
- [42] René Ranftl, Katrin Lasinger, David Hafner, Konrad Schindler, and Vladlen Koltun. Towards robust monocular depth estimation: Mixing datasets for zero-shot cross-dataset transfer. *IEEE TPAMI*, 44(3):1623–1637, 2020. **8**
- [43] Nikhila Ravi, Jeremy Reizenstein, David Novotny, Taylor Gordon, Wan-Yen Lo, Justin Johnson, and Georgia Gkioxari. Accelerating 3d deep learning with pytorch3d. *arXiv preprint arXiv:2007.08501*, 2020. **6**
- [44] Shaoqing Ren, Kaiming He, Ross Girshick, and Jian Sun. Faster r-cnn: Towards real-time object detection with region proposal networks. *IEEE TPAMI*, 39(6):1137–1149, 2016. **1, 3, 4**
- [45] Mike Roberts, Jason Ramapuram, Anurag Ranjan, Atulit Kumar, Miguel Angel Bautista, Nathan Paczan, Russ Webb, and Joshua M Susskind. Hypersim: A photorealistic synthetic dataset for holistic indoor scene understanding. In *ICCV*, 2021. **5**
- [46] Danila Rukhovich, Anna Vorontsova, and Anton Konushin. Imvoxelnet: Image to voxels projection for monocular and multi-view general-purpose 3d object detection, 2021. **2**
- [47] Danila Rukhovich, Anna Vorontsova, and Anton Konushin. Imvoxelnet: Image to voxels projection for monocular and multi-view general-purpose 3d object detection. In *Proceedings of the IEEE/CVF Winter Conference on Applications of Computer Vision*, 2022. **1**
- [48] Olga Russakovsky, Jia Deng, Hao Su, Jonathan Krause, Sanjeev Satheesh, Sean Ma, Zhiheng Huang, Andrej Karpathy, Aditya Khosla, Michael Bernstein, et al. Imagenet large scale visual recognition challenge. *International journal of computer vision*, 115:211–252, 2015. **2**
- [49] Shuai Shao, Zeming Li, Tianyuan Zhang, Chao Peng, Gang Yu, Xiangyu Zhang, Jing Li, and Jian Sun. Objects365: A large-scale, high-quality dataset for object detection. In *ICCV*, 2019. **1, 2**
- [50] Andrea Simonelli, Samuel Rota Buló, Lorenzo Porzi, Manuel López-Antequera, and Peter Kontschieder. Disentangling monocular 3D object detection. In *ICCV*, 2019. **4**
- [51] Shuran Song, Samuel P Lichtenberg, and Jianxiong Xiao. Sun rgb-d: A rgb-d scene understanding benchmark suite. In *CVPR*, 2015. **5, 3**
- [52] Tai Wang, Xinge Zhu, Jiangmiao Pang, and Dahua Lin. Fcos3d: Fully convolutional one-stage monocular 3d object detection, 2021. **2**
- [53] Tai Wang, ZHU Xinge, Jiangmiao Pang, and Dahua Lin. Probabilistic and geometric depth: Detecting objects in perspective. In *Conference on Robot Learning*, pages 1475–1485. PMLR, 2022. **1, 2**
- [54] Zhenyu Wang, Yali Li, Taichi Liu, Hengshuang Zhao, and Shengjin Wang. Ov-uni3detr: Towards unified open-vocabulary 3d object detection via cycle-modality propagation. *arXiv preprint arXiv:2403.19580*, 2024. **2**
- [55] Size Wu, Wenwei Zhang, Lumin Xu, Sheng Jin, Wentao Liu, and Chen Change Loy. Clim: Contrastive language-image mosaic for region representation. In *AAAI*, pages 6117–6125, 2024. **1**
- [56] Yuxin Wu, Alexander Kirillov, Francisco Massa, Wan-Yen Lo, and Ross Girshick. Detectron2. <https://github.com/facebookresearch/detectron2>, 2019. **6**
- [57] Alireza Zareian, Kevin Dela Rosa, Derek Hao Hu, and Shih-Fu Chang. Open-vocabulary object detection using captions. In *CVPR*, 2021. **2**
- [58] Dongmei Zhang, Chang Li, Renrui Zhang, Shenghao Xie, Wei Xue, Xiaodong Xie, and Shanghang Zhang. Fm-ov3d:

- Foundation model-based cross-modal knowledge blending for open-vocabulary 3d detection. In *AAAI*, 2024. 2
- [59] Hao Zhang, Feng Li, Shilong Liu, Lei Zhang, Hang Su, Jun Zhu, Lionel M Ni, and Heung-Yeung Shum. Dino: Detr with improved denoising anchor boxes for end-to-end object detection. *arXiv preprint arXiv:2203.03605*, 2022. 4
- [60] Haotian Zhang, Pengchuan Zhang, Xiaowei Hu, Yen-Chun Chen, Liunian Li, Xiyang Dai, Lijuan Wang, Lu Yuan, Jenq-Neng Hwang, and Jianfeng Gao. Glipv2: Unifying localization and vision-language understanding. *NeurIPS*, 2022. 2
- [61] Hu Zhang, Jianhua Xu, Tao Tang, Haiyang Sun, Xin Yu, Zi Huang, and Kaicheng Yu. Opensight: A simple open-vocabulary framework for lidar-based object detection. In *ECCV*. Springer, 2025. 2
- [62] Junyi Zhang, Charles Herrmann, Junhwa Hur, Luisa Polania Cabrera, Varun Jampani, Deqing Sun, and Ming-Hsuan Yang. A tale of two features: Stable diffusion complements dino for zero-shot semantic correspondence. *NeurIPS*, 2024. 7
- [63] Renrui Zhang, Ziyu Guo, Wei Zhang, Kunchang Li, Xupeng Miao, Bin Cui, Yu Qiao, Peng Gao, and Hongsheng Li. Pointclip: Point cloud understanding by clip. In *Proceedings of the IEEE/CVF conference on computer vision and pattern recognition*, pages 8552–8562, 2022. 2
- [64] Renrui Zhang, Han Qiu, Tai Wang, Ziyu Guo, Ziteng Cui, Yu Qiao, Hongsheng Li, and Peng Gao. Monodetr: Depth-guided transformer for monocular 3d object detection. In *ICCV*, pages 9155–9166, 2023. 2
- [65] Chong Zhou, Chen Change Loy, and Bo Dai. Extract free dense labels from clip. In *ECCV*, pages 696–712. Springer, 2022. 1
- [66] Dingfu Zhou, Xibin Song, Yuchao Dai, Junbo Yin, Feixiang Lu, Jin Fang, Miao Liao, and Liangjun Zhang. Iafa: Instance-aware feature aggregation for 3d object detection from a single image, 2021. 2
- [67] Xingyi Zhou, Dequan Wang, and Philipp Krähenbühl. Objects as points, 2019. 2
- [68] Xingyi Zhou, Rohit Girdhar, Armand Joulin, Philipp Krähenbühl, and Ishan Misra. Detecting twenty-thousand classes using image-level supervision. In *European Conference on Computer Vision*, pages 350–368. Springer, 2022. 2
- [69] Yi Zhou, Connelly Barnes, Jingwan Lu, Jimei Yang, and Hao Li. On the continuity of rotation representations in neural networks. In *CVPR*, 2019. 3
- [70] Chenming Zhu, Wenwei Zhang, Tai Wang, Xihui Liu, and Kai Chen. Object2scene: Putting objects in context for open-vocabulary 3d detection. *arXiv preprint arXiv:2309.09456*, 2023. 2

Open Vocabulary Monocular 3D Object Detection

Supplementary Material

Sec. A presents per-category performance on novel classes in 2D and 3D for OVMONO3D-GEO and OVMONO3D-LIFT. Sec. B provides additional qualitative visualizations on various datasets and compares predictions between OVMONO3D-GEO and OVMONO3D-LIFT. Sec. C discusses failure cases, highlighting challenges such as occlusions, out-of-distribution objects, and small or distant instances.

A. Per-category Performance on novel classes

We show per-category performance on Average Precision (AP) and Average Recall (AR) on both 2D and 3D for OVMONO3D-GEO and OVMONO3D-LIFT in Tabs. 8 and 9, respectively.

| Category | AP _{2D} | AP _{3D} | AR _{2D} | AR _{3D} |
|------------------------|------------------|------------------|------------------|------------------|
| Board | 29.41 | 2.06 | 34.05 | 7.78 |
| Printer | 31.05 | 8.96 | 41.77 | 22.99 |
| Painting | 33.39 | 2.09 | 44.80 | 9.04 |
| Microwave | 31.60 | 14.06 | 39.45 | 28.27 |
| Tray | 15.65 | 3.40 | 22.30 | 13.11 |
| Podium | 46.66 | 36.71 | 53.85 | 46.92 |
| Cart | 31.49 | 32.52 | 38.25 | 41.75 |
| Tram | 4.72 | 0.61 | 6.91 | 1.58 |
| <i>Easy Categories</i> | 28.00 | 12.55 | 35.17 | 21.43 |
| Monitor | 18.84 | 6.55 | 30.02 | 19.36 |
| Bag | 13.98 | 8.20 | 23.46 | 21.45 |
| Dresser | 27.43 | 14.87 | 38.22 | 30.86 |
| Keyboard | 12.06 | 7.23 | 25.41 | 18.56 |
| Drawers | 19.87 | 9.29 | 32.67 | 21.42 |
| Computer | 15.73 | 5.73 | 25.00 | 19.70 |
| Kitchen Pan | 5.56 | 7.36 | 14.22 | 16.67 |
| Potted Plant | 15.05 | 10.65 | 28.06 | 27.10 |
| Tissues | 5.88 | 3.04 | 11.55 | 9.86 |
| Rack | 9.19 | 3.54 | 12.50 | 8.17 |
| Toys | 10.35 | 8.84 | 21.94 | 19.17 |
| Phone | 3.30 | 5.00 | 9.52 | 12.62 |
| Soundssystem | 13.09 | 7.43 | 20.47 | 19.53 |
| Fireplace | 17.48 | 0.42 | 39.51 | 3.86 |
| <i>Hard Categories</i> | 13.42 | 7.01 | 23.75 | 17.74 |
| <i>All Categories</i> | 18.72 | 9.03 | 27.91 | 19.08 |

Table 8. Per-category Performance of OVMONO3D-GEO.

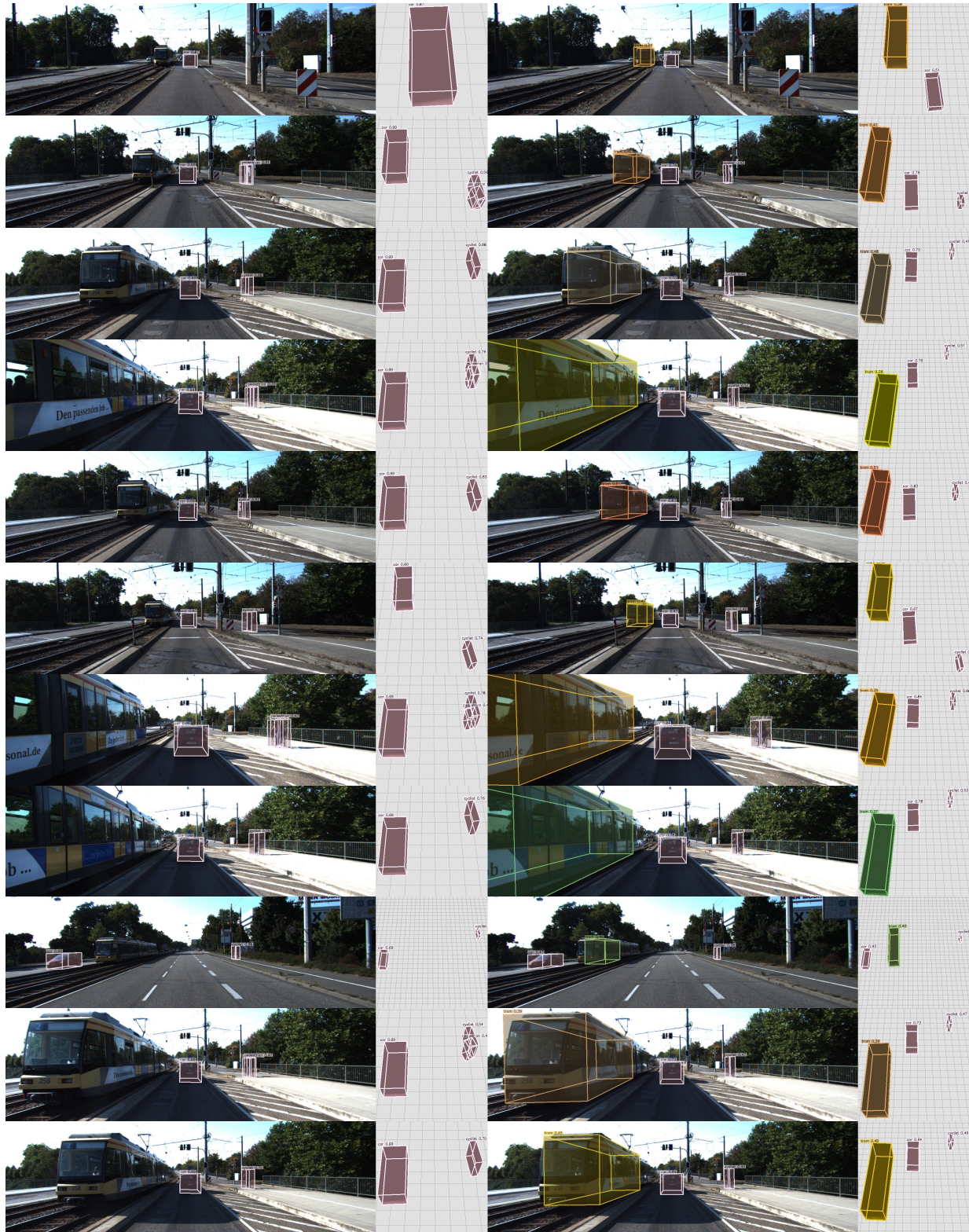
B. More Qualitative Results

Additional qualitative visualizations of OVMONO3D-LIFT are provided for Omni3D [5] outdoor, indoor subsets, and COCO [31] in-the-wild images in Figs. 8 to 10, respectively.

Fig. 11 illustrates a comparison between the predictions of OVMONO3D-GEO and OVMONO3D-LIFT. OVMONO3D-GEO derives object depth from an estimated metric depth map, yielding better relative depth consistency with scene layout (e.g., Fig. 11c). However, it estimates dimensions and poses based on visible object parts, leading to biases. For instance, it struggles with occlusions (e.g., the door in Fig. 11d), limited surface visibility (e.g., ovens in Fig. 11e), and noisy depth maps (e.g., the farthest chair in Fig. 11f). In contrast, OVMONO3D-LIFT, leveraging learned priors, is more robust in such scenarios. Future work could integrate these methods to mitigate their respective limitations.

| Category | AP _{2D} | AP _{3D} | AR _{2D} | AR _{3D} |
|------------------------|------------------|------------------|------------------|------------------|
| Board | 38.90 | 4.83 | 54.51 | 20.52 |
| Printer | 31.02 | 16.23 | 44.08 | 43.95 |
| Painting | 34.99 | 2.80 | 50.23 | 19.77 |
| Microwave | 32.76 | 30.31 | 42.91 | 56.27 |
| Tray | 17.75 | 10.11 | 32.79 | 30.16 |
| Podium | 45.63 | 48.37 | 57.18 | 73.08 |
| Cart | 37.54 | 47.31 | 50.75 | 71.50 |
| Tram | 22.86 | 4.71 | 34.00 | 9.15 |
| <i>Easy Categories</i> | 32.68 | 20.58 | 45.81 | 40.55 |
| Monitor | 21.46 | 9.44 | 38.64 | 35.44 |
| Bag | 15.90 | 15.61 | 30.22 | 36.42 |
| Dresser | 30.54 | 29.08 | 48.49 | 60.26 |
| Keyboard | 14.60 | 9.13 | 36.71 | 25.07 |
| Drawers | 21.48 | 43.04 | 43.00 | 68.33 |
| Computer | 16.80 | 7.44 | 35.30 | 28.56 |
| Kitchen Pan | 6.81 | 9.98 | 21.57 | 35.10 |
| Potted Plant | 12.94 | 6.66 | 33.23 | 24.62 |
| Tissues | 8.81 | 12.45 | 21.55 | 32.68 |
| Rack | 13.02 | 10.21 | 27.33 | 35.33 |
| Toys | 10.91 | 5.24 | 29.31 | 22.08 |
| Phone | 6.23 | 3.89 | 22.14 | 16.43 |
| Soundssystem | 14.52 | 13.22 | 31.86 | 31.86 |
| Fireplace | 19.50 | 13.16 | 47.62 | 34.06 |
| <i>Hard Categories</i> | 15.25 | 13.47 | 33.36 | 34.73 |
| <i>All Categories</i> | 21.59 | 16.05 | 37.88 | 36.85 |

Table 9. Per-category Performance of OVMONO3D-LIFT.



Cube R-CNN

OVMono3D-LIFT

Figure 8. **Qualitative Visualizations on the KITTI [15] Test Set.** For each example, we present the predictions of Cube R-CNN [5] and OVMONO3D-LIFT, displaying both the 3D predictions overlaid on the image and a top-down view with a base grid of $1\text{ m} \times 1\text{ m}$ tiles. Base categories are depicted with brown cubes, while novel categories are represented in other colors.



Figure 9. **Qualitative Visualizations on the SUN RGB-D [51] Test Set.** For each example, we present the predictions of Cube R-CNN [5] and OVMONO3D-LIFT, displaying both the 3D predictions overlaid on the image and a top-down view with a base grid of $1\text{ m} \times 1\text{ m}$ tiles. Base categories are depicted with brown cubes, while novel categories are represented in other colors.

C. Failure Cases

Fig. 12 shows failure cases of OVMONO3D-LIFT on COCO [31] images. In Fig. 12a, the relative position from a top-down view is incorrect, indicating that our model sometimes predicts the wrong object depth. In Fig. 12b, our model fails to predict the correct size and pose for the bear, suggesting that it may struggle with totally out-of-distribution objects. In Fig. 12c, our model fails to detect the person and bus in the distance, indicating that it may not perform well on small and distant objects. In Fig. 12d, our method fails to identify the mirror and incorrectly detects

the object in the mirror. These failure cases suggest that our model still has room for improvement. Future research could explore better model architectures and weakly supervised learning techniques to address these shortcomings.



Figure 10. **OVMONO3D-LIFT on In-the-Wild COCO [31] Images.** We display 3D predictions overlaid on the images and the top-down views with a base grid of $1\text{ m} \times 1\text{ m}$ tiles.

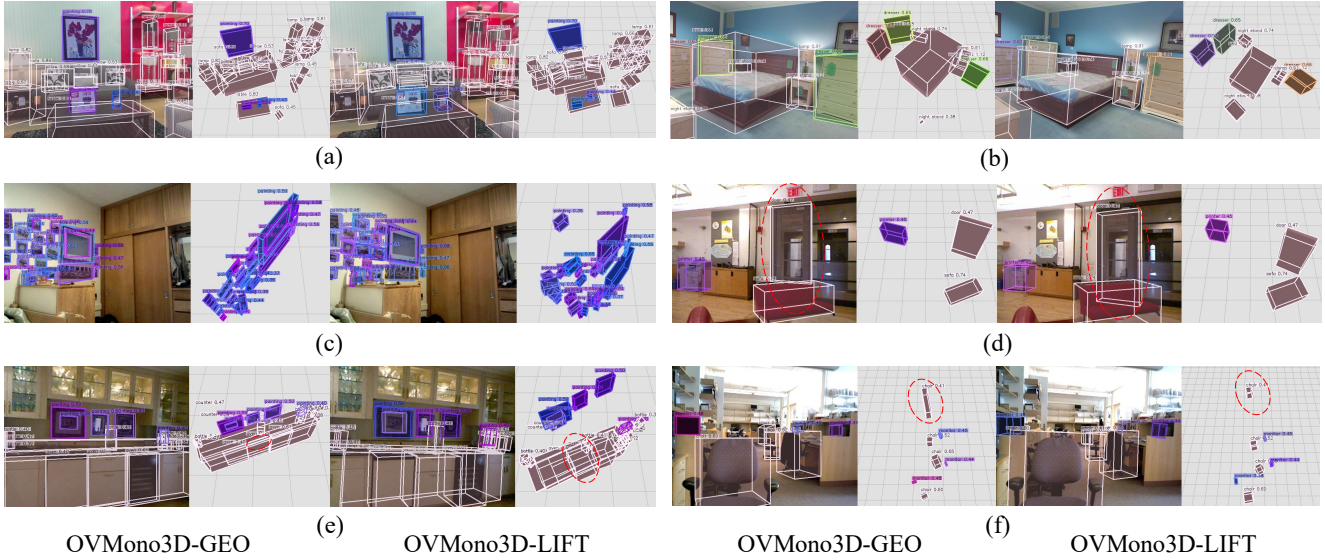


Figure 11. **OVMONO3D-GEO vs. OVMONO3D-LIFT on SUN RGB-D [51] Images.** For each example, we display the predictions of OVMONO3D-GEO and OVMONO3D-LIFT. We display 3D predictions overlaid on the images and the top-down views with a base grid of $1\text{ m} \times 1\text{ m}$ tiles. Base categories are depicted with brown cubes, while novel categories are represented in other colors.

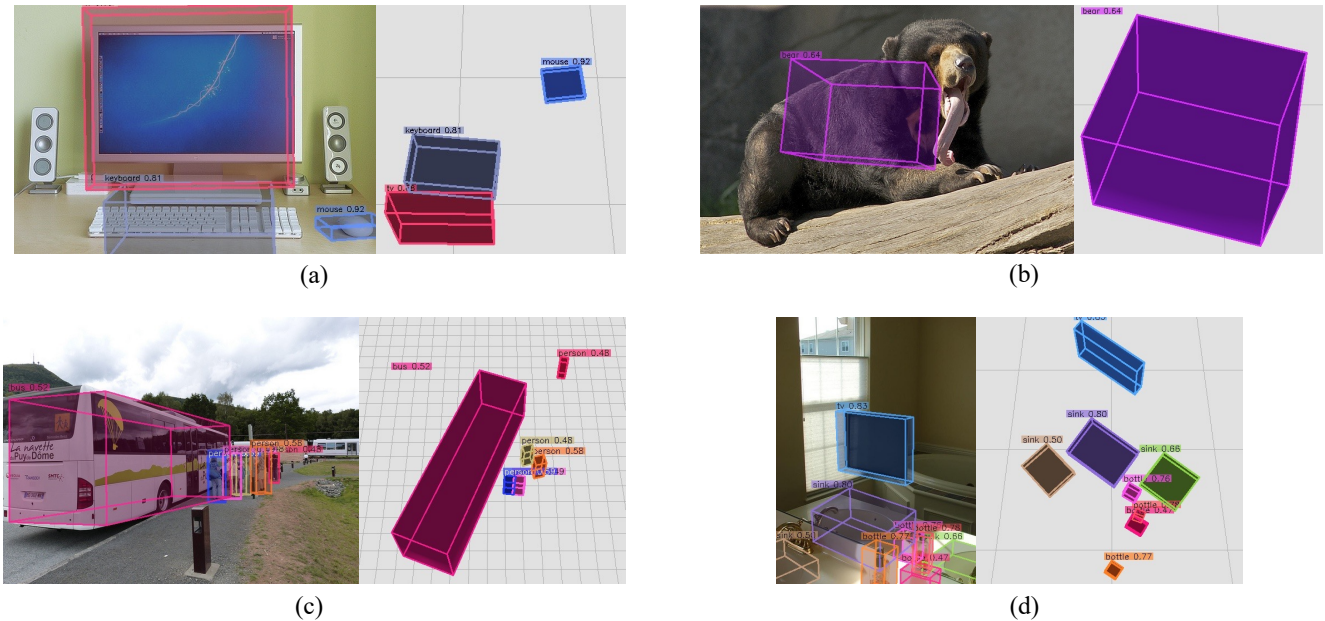


Figure 12. **Failure Cases of OVMONO3D-GEO on COCO [31] Images.** We display 3D predictions overlaid on the images and the top-down views with a base grid of $1\text{ m} \times 1\text{ m}$ tiles.